Electronic Supplementary Material (ESI) for Soft Matter.

Ellipsoidal Particles Encapsulated in Droplets

Supporting Information

Michael M. Norton*, Teresa Brugarolas**, Jonathan Chou**, Daeyeon Lee**, and Haim Bau*
* Mechanical Engineering and Applied Mechanics
** Chemical and Biomolecular Engineering
University of Pennsylvania, Philadelphia PA USA

S1. Drop shape calculation using energy minimization

To enable the calculation of the drop shape under conditions of non-constant curvature (i.e., when one wishes to account for Van der Waals forces), we developed an algorithm based on the minimization of the free energy. In this section, we briefly describe the energy minimization algorithm and verify its performance by comparing its predictions with unduloid-based solutions.

We define the functional

$$F = E_{\alpha\beta} + E_{\alpha\sigma} + E_{\beta\sigma} + E_v \tag{S1}$$

where

$$E_{\alpha\beta} = \gamma_{\alpha\beta} 2\pi \int_{\phi_1}^{\frac{\pi}{2}} \rho_{\alpha\beta} \sqrt{\left(\frac{\mathrm{d}\rho_{\alpha\beta}}{\mathrm{d}\phi}\right)^2 + \rho_{\alpha\beta}^2}\, \sin\phi\, \mathrm{d}\phi \tag{S2}$$

is the surface energy of the droplet-continuous phase ($\alpha\beta$) interface;

$$E_{\alpha\sigma} = \gamma_{\alpha\sigma} 2\pi \int_{\phi_1}^{\frac{\pi}{2}} \rho_{\alpha\sigma} \sqrt{\left(\frac{\mathrm{d}\rho_{\alpha\sigma}}{\mathrm{d}\phi}\right)^2 + \rho_{\alpha\sigma}^2}\, \sin\phi\, \mathrm{d}\phi \tag{S3}$$

is the surface energy of the droplet-solid ($\alpha\sigma$) interface;

$$E_{\beta\sigma} = \gamma_{\beta\sigma} 2\pi \int_{0}^{\phi_1} \rho_{\beta\sigma} \sqrt{\left(\frac{\mathrm{d}\rho_{\beta\sigma}}{\mathrm{d}\phi}\right)^2 + \rho_{\beta\sigma}^2}\, \sin\phi\, \mathrm{d}\phi \tag{S4}$$

is the surface energy of the continuous phase-solid ($\beta\sigma$) interface; and

$$E_v = \lambda\left[\frac{2\pi}{3}\int_{\phi_1}^{\frac{\pi}{2}}(\rho_{\alpha\beta}^3 - \rho_{\alpha\sigma}^3)\sin\phi\,\mathrm{d}\phi - \frac{V}{2}\right] \qquad \text{(S5)}$$

is the volume constraint. All are written in spherical coordinates defined in Fig. 3. The volume constraint is enforced through the Lagrange multiplier λ that corresponds to the static (Laplace) pressure in α. In all the above equations, integration about the azimuthal angle has already been carried out. The task is to determine the shape of the ($\alpha\beta$) interface $\rho_{\alpha\beta}(\phi)$ and the position of the contact line ϕ_1 that minimizes F.

Although the contact angle θ does not appear explicitly in equations S1-S5, the state that minimizes F satisfies Young's equation. To see this, we consider one of the essential conditions of the stationary state:

$$\frac{\partial F}{\partial \phi_1} = 0\,. \qquad \text{(S6)}$$

Since $\partial E_V / \partial \phi_1 = 0$, we have

$$\frac{\partial E_{\alpha\beta}}{\partial \phi_1} + \frac{\partial E_{\alpha\sigma}}{\partial \phi_1} + \frac{\partial E_{\beta\sigma}}{\partial \phi_1} = 0\,. \qquad \text{(S7)}$$

Further, since $\rho_e \equiv \rho_{\beta\sigma}(\phi_1) = \rho_{\alpha\sigma}(\phi_1) = \rho_{\alpha\beta}(\phi_1)$, we have:

$$\gamma_{\alpha\sigma} - \gamma_{\beta\sigma} + \frac{\left.\sqrt{\left(\frac{\mathrm{d}\rho_{\alpha\beta}}{\mathrm{d}\phi}\right)^2 + \rho_e^2}\right|_{\phi_1}}{\left.\sqrt{\left(\frac{\mathrm{d}\rho_e}{\mathrm{d}\phi}\right)^2 + \rho_e^2}\right|_{\phi_1}}\gamma_{\alpha\beta} = 0\,. \qquad \text{(S8)}$$

The term in front of $\gamma_{\alpha\beta}$ is a ratio of arc-lengths and can be replaced with the cosine of the contact angle to retrieve the Young's equation:

$$\gamma_{\alpha\sigma} - \gamma_{\beta\sigma} + \gamma_{\alpha\beta}\cos\theta = 0\,. \qquad \text{(S9)}$$

To minimize F, we resort to numerical techniques. The interface αβ is divided into N segments each having an arc length l (see Fig. 3). l is not known *a priori* and must be determined

as part of the solution. The restriction of uniform segments is enforced with an additional pseudo-energy term:

$$E_l = \sum_{n=1}^{N-1} \eta_n \left[\left(\rho_{\alpha\beta;n+1} - \rho_{\alpha\beta;n} \right)^2 + \rho_{\alpha\beta;n} \left(\phi_{n+1} - \phi_n \right)^2 - l^2 \right]. \quad \text{(S10)}$$

The above constraint prevents the nodes from aggregating in a narrow region. In Fig. 3, nodes are labeled with hollow circles and the nth node is highlighted with a solid circle. Node n=1 corresponds with the contact line. At the contact line, ϕ_1 is to be determined while ρ_1 is available from the particle's geometry. The left-right symmetry is enforced by fixing $\phi_N = \pi/2$. The discretized equations are:

$$E_v = \lambda \left\{ \frac{\pi}{3} \sum_{n=1}^{N-1} \left[\sin\phi_{n+1} \left(\rho_{\alpha\beta;n+1}^3 - \rho_{\alpha\sigma;n+1}^3 \right) + \sin\phi_n \left(\rho_{\alpha\beta;n}^3 - \rho_{\alpha\sigma;n}^3 \right) \right] \left(\phi_{n+1} - \phi_n \right) - \frac{V}{2} \right\} \quad \text{(S11)}$$

and

$$E_{\alpha\beta} = 2\pi\gamma_{\alpha\beta} \sum_{n=1}^{N-1} l\rho_{\alpha\beta;n} \sin\phi_n . \quad \text{(S12)}$$

We find the stationary state by setting the derivatives of the energy functional with respect to all degrees of freedom **x** to zero.

$$\frac{\partial F}{\partial \mathbf{x}} = 0 . \quad \text{(S13)}$$

In the above,

$$\mathbf{x} = \left[\left(\rho_2, \rho_3 \ldots \rho_N \right), \left(\phi_1, \phi_2 \ldots \phi_{N-1} \right), \left(\eta_1, \eta_2 \ldots \eta_{N-1} \right), \lambda, l \right]. \quad \text{(S14)}$$

We solve equation S13 with the Newton-Raphson method

$$\mathbf{x}^{(k+1)} = \mathbf{x}^{(k)} - \left[\left(\frac{\partial^2 F}{\partial \mathbf{x} \partial \mathbf{x}} \right)^{-1} \right]^{(k)} \frac{\partial F}{\partial \mathbf{x}}^{(k)} . \quad \text{(S15)}$$

In the above, the superscript denotes the k^{th} iterate. The first order derivatives and Jacobian matrix were determined analytically. The corresponding expressions are lengthy and therefore not reproduced here.

Typically $N \sim 100$ nodes were sufficient to achieve grid-independence. The energy minimization code was verified by reproducing known solutions for the cylindrical fiber wetting problem [S1]. Fig. S1A compares the energy-minimization solution (hollow circles) with the analytical solution (solid line) when $\theta = 45^{\circ}$. Fig. S1B depicts the relative discrepancy between the analytical solution and the energy minimization solution for the position of the droplet apex (squares) and droplet pinning point (circles) as functions of the number of nodes (N). When N>80, the error is smaller than 1%.

Next, we applied the energy minimization algorithm to determine the shape of a drop partially engulfing an ellipsoidal particle. Figs. S2A and S2B depict, respectively, z_1^* and r_2^* as functions of the volume as determined by the energy minimization method (solid circles) and the unduloid solution (solid lines). ε=5 and $\theta = 90^{\circ}$. Both solution methods produced nearly identical results. To illustrate the convexity of the energy functional, Fig. S3 depicts the free energy of a fixed volume drop as a function of the pinning line position ϕ_1 for various contact angles.

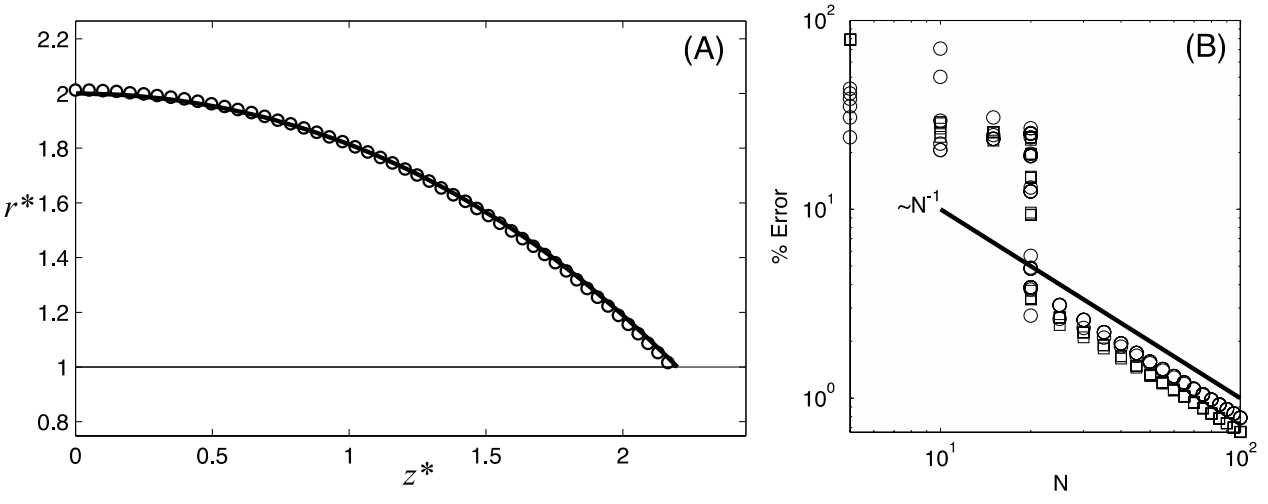

Fig. S1: (A) The shape of a drop wetting a cylindrical fiber [12] as obtained with the unduloid method (solid line) and the energy minimization method (hollow circles, N=100, not all nodes are plotted). $\theta = 45^{\circ}$. (B) The relative discrepancy between the energy minimization and the unduloid predictions of the droplet apex (squares) and the axial position of the pinning point (circles) as a function of the number of nodes (N) used in the discretization of the drop surface; for large *N,* the error decreases as N^{-1}.

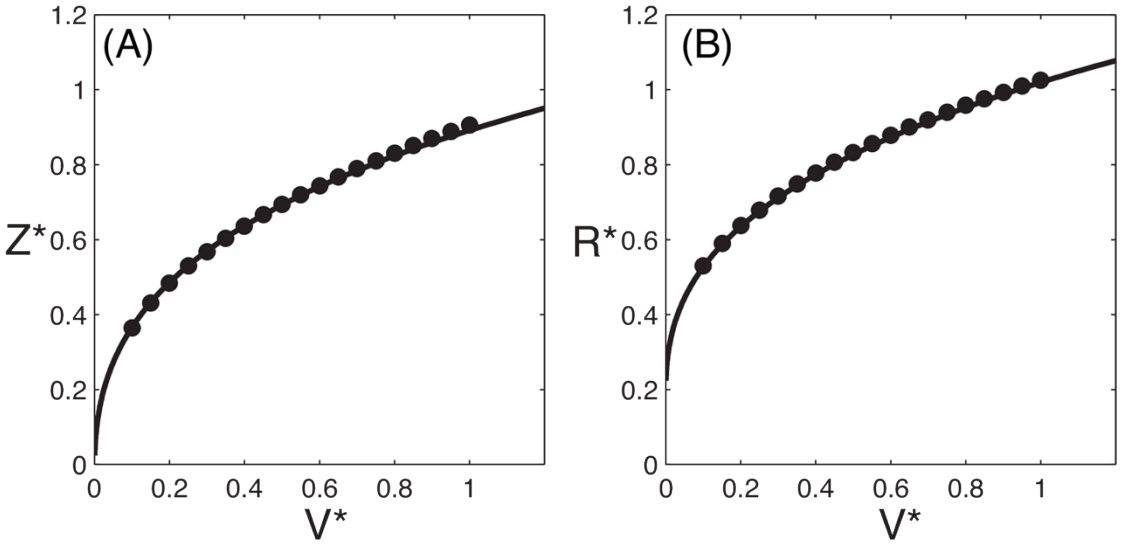

Figure S2: The axial position of the pinning line (A) and the drop radius $r_2^* / \varepsilon = r_2 / a$ (B) as functions of the dimensionless volume V^*. The solid lines and the symbols denote, respectively, the unduloid solution [S1] and the energy minimization solution. ε=5 and $\theta = 90^\circ$.

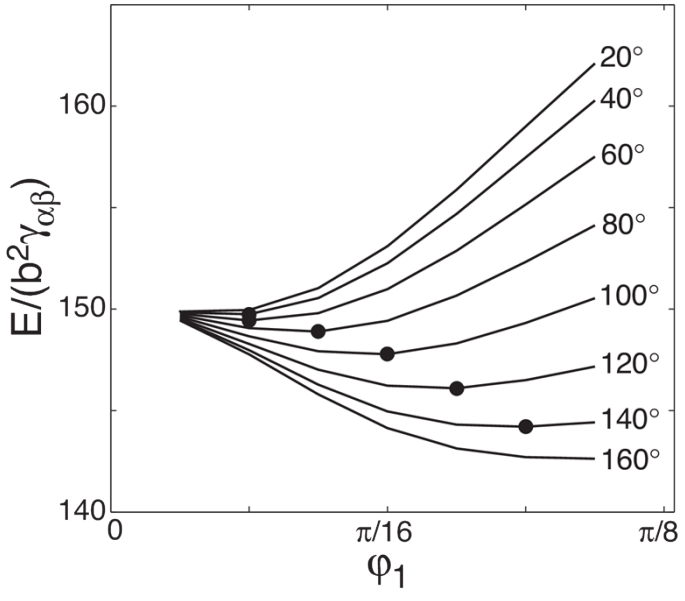

Figure S3: The penalty function (S1) as a function of the pinning line position ϕ_1 for various contact angles. □=3. The energy minima, when present, are denoted with solid circles.

S2. Contact Angle Measurement

The three-phase contact angle was measured by an ex-situ experiment using a planar polystyrene film. A concentrated solution of polystyrene in toluene (20% w/v) was spin coated onto a glass slide with a commercial spin coater (Laurell Technologies Co., WS-400BZ-6NPP/Lite). The presence of PVA during the microfluidic generation of the polystyrene particles and the stretching of the particles into ellipsoids was simulated by spin coating 2% w/w PVA in water onto the PS film, followed by three subsequent spin coatings of water to rinse off any excess PVA. The composed film was heated to above the glass transition temperature (100^{o}C) of Polystyrene using a hot plate [S8]. The film was rinsed with DI water and air dried before the contact angle measurement.

The three phase contact angle was measured with a goniometer (Theta Optical Tensiometer, Attension KSV instruments). The continuous phase consists of DI water and the dispersed phase of light mineral oil containing a 5% v/v surfactant ABIL EM 90 (Evonik Industries). The average contact angle obtained from four different samples prepared in a similar manner was $165.8 \pm 5.2^{\circ}$, which confirmed the hydrophilic character of the treated polystyrene. The contact angle of interest in our work is the supplementary angle $14.2 \pm 5.2^{\circ}$.

S3. Dimensionless Groups

In the manuscript, we introduced several dimensionless groups to justify our assumptions. The various material properties used in these calculations are listed in Table S1. The relevant length and velocity scales are tabulated in Table S2 and the values for the dimensionless groups in Table S3. The smaller the magnitude of the dimensionless group , the more the interfacial tension forces dominate the system's behavior.

For the elastic modulus of *C.elegans,* we used the conservative value of 3.77 kPa [S4]. Other sources indicate higher elastic moduli for nematodes such as 50 kPa [S5] and 380 MPa [S6] for the cuticle.

parameter	value
ϱ_α	1.00e3 [kg/m^3]
ϱ_β	8.3e2 [kg/m^3]
μ_α	1e-3 [Pa s]
μ_β	2.78e-2 [Pa s]
$\gamma_{\alpha\beta}$	1e-3 [N/m] [S3, S2]
E_{CE}	3.77e-1[Pa] [S4]
E_{PS}	3.6e9 [Pa] [S7]

Table S1: The magnitudes of the various properties used in the calculation of Table S3. The light mineral oil's manufacturer provides the kinematic viscosity at 40^{o}C while the specific gravity is given at 15.6^{o}C. Subscripts *CE* and *PS,* respectively, denote properties of the *C.elegans* and polystyrene.

parameter	value
$r_{2,D}$	5e-4 [m]
U	6e-3[m/s]
a_{CE}	4e-5 [m]
$2b_{CE}$	1.13e-3 [m]
a_{PS}	5e-5 [m]
$2b_{PS}$	7e-4 [m]

Table S2: Typical velocity and length scales. Subscripts D, CE, and PS denote properties belonging to a typical droplet, *C.elegans*, or polystyrene particle.

quantity	value
Bo	4.17e-1
Ca_o	1.67e-1
We	1.80e-2
Γ_{CE}	1.07e6
Γ_{PS}	2.21e-7

Table S3: Estimated magnitudes of the non-dimensional parameters relevant to our system

S4. How ellipsoidal is the particle?

As a matter of convenience, in the manuscript, we assumed the particles have an ellipsoidal shape. To assess the accuracy of our assumption, we compare the profile of several particles to an analytical expression for ellipsoids. The profile is obtained by manually selecting $N\sim50$ points

along the surface of an imaged particle in ImageJ. The major and minor axes for the analytical expression are acquired by circumscribing an ellipse around the particle in ImageJ and matching the narrowest and widest portions of the particle. We use polar coordinates to calculate the error metric:

$$\sqrt{\frac{1}{N}\sum_{i=1}^{N}\left(\frac{\rho_{\text{ellipse,i}}-\rho_{\text{exp.,i}}}{\varepsilon}\right)^2}, \qquad \text{(S16)}$$

Five particles were measured; the maximum deviation between the ellipsoids and the actual particles was 3.8%.

REFERENCES

[S1] B. J. Carroll. Accurate measurement of contact-angle, phase contact areas, drop volume, and laplace excess pressure in drop-on-fiber systems. *Journal of Colloid and Interface Science*, 57(3):488–495, 1976. Cp389 Times Cited:175 Cited References Count:10.

[S2] A. S. Utada, A. Fernandez-Nieves, H. A. Stone, and D. A. Weitz. Dripping to jetting transitions in coflowing liquid streams. *Physical Review Letters*, 99(9), 2007. 206AE Times Cited:121 Cited References Count:31.

[S3] A. S. Utada, E. Lorenceau, D. R. Link, P. D. Kaplan, H. A. Stone, and D. A. Weitz. Monodisperse double emulsions generated from a microcapillary device. *Science*, 308(5721):537–

[S4] J. Sznitman, P. K. Purohit, P. Krajacic, T. Lamitina, and P. E. Arratia. Material properties of caenorhabditis elegans swimming at low reynolds number. *Biophysical Journal*, 98(4):617–626, 2010.

[S5] S. J. Park, M. B. Goodman, and B. L. Pruitt. Measurement of mechanical properties of caenorhabditis elegans with a piezoresistive microcantilever system. *2005 3rd IEEE/EMBS Special Topic Conference on Microtechnology in Medicine and Biology*, pages 400–403, 2005.

[S6] S. J. Park, M. B. Goodman, and B. L. Pruitt. Analysis of nematode mechanics by piezoresistive displacement clamp. *Proceedings of the National Academy of Sciences of the United States of America*, 104(44):17376–17381, 2007.

[S7] C. M. Stafford, B. D. Vogt, C. Harrison, D. Julthongpiput, and R. Huang. Elastic moduli of ultrathin amorphous polymer films. *Macromolecules*, 39(15):5095–5099, 2006.

[S8] J. C. Loudet, A. G. Yodh, and B. Pouligny. Wetting and contact lines of micrometer-sized ellipsoids. *Physical Review Letters*, 97(1), 2006.